공학석사 학위논문

Bacterial inactivation by visible light-activated ZIF-8: Bactericidal mechanism revisited

금속 유기 골격체 ZIF−8의 가시광촉매적
항균 특성 및 세균 불활성화 기작 연구

2023년 2월

서울대학교 대학원
공과대학 화학생물공학부 화학생물공학 전공
박 도 연

Bacterial inactivation by visible light-activated ZIF-8: Bactericidal mechanism revisited

지도 교수 이 창 하

이 논문을 공학석사 학위논문으로 제출함
2022년 12월

서울대학교 대학원
공과대학 화학생물공학부 화학생물공학 전공
박 도 연

박도연의 공학석사 학위논문을 인준함
2023년 1월

위 원 장	남 재 욱	(인)
부위원장	이 창 하	(인)
위 원	강 종 헌	(인)

Abstract

Bacterial inactivation by visible light-activated ZIF-8: Bactericidal mechanism revisited

Doyeon Park

School of Chemical and Biological Engineering

The Graduate School

Seoul National University

Metal-organic frameworks (MOFs) have attracted considerable attention as versatile materials applicable in a variety of areas including biomedical and environmental applications. Among various MOFs, ZIF-8 has been extensively studied to achieve disinfection activity. Despite of the wide range of previous work, little is known about the bactericidal mechanism of ZIF-8. It has been suggested that the precursors of ZIF-8 are responsible for *E. coli* inactivation, but these claims are questionable. Meanwhile, a literature has shown that ZIF-8 has excellent activity for the photocatalytic inactivation of *E. coli*, although the photo-enhanced activity of ZIF-8 under visible light has not been studied. This study firstly declared visible light-enhanced inactivation ability of ZIF-8, which cannot be explained by the large band gap of ZIF-8. Based on the results, the formation of Zn-mim-bacteria complex

is regarded as the main cause of the bacterial disinfection, inducing synergistic bactericidal activity. Additional UV-Vis DRS peak of the complex was observed in the visible light region, indicating new photo-activity generated by the complex formation. The possible bactericidal actions generated by photo-activated ZIF-8 were discussed in this paper.

Keyword : ZIF-8, Visible light illumination, Bactericidal activity, Metal-organic frameworks (MOFs), Photoenhanced, Disinfection

Student Number : 2021-27894

Contents

List of Figures

1. Introduction

Various pathogenic microorganisms present in human daily lives, threatening public health through water, air, and surface contamination. Waterborne diseases, in particular, are concerned as serious problem for public health. Water contamination encompasses illness resulting from exposure to water, associated with high morbidity and mortality. About 1.5 million people died from diarrheal diseases in 2019, which are mostly caused by poor water sanitation (WHO, 2022).

Conventional disinfection system mostly relies on chemical oxidation in homogeneous system, using strong oxidants such as chlorine-based products and ozone. Despite their wide use, many studies have reported that harmful disinfection byproducts (DBPs) such as trihalomethanes, aldehydes, and bromates can be formed during the procedure (Gopal et al., 2007; Huang et al., 2005; Nieuwenhuijsen et al., 2000). Since these DBPs are hard to control and highly toxic, alternative disinfection methods are strongly demanded to solve the problem. Bacterial resistance and inefficient disinfection of newly emerging pathogens are also an important issue of the current system (Martínez-Huitle and Brillas, 2021). Hence, a number of studies have been developing new approaches to avoid the suggested problems.

Among the alternatives, heterogeneous materials gained considerable attention in recent years. Metal ion, organic or inorganic materials, photocatalytic semiconductors are used to improve antimicrobial efficiency. Recently, there has been extensive research about metal organic frameworks (MOFs) in many fields including environmental and biomedical area (Li et al., 2021; Yang and Yang, 2020). MOFs have drawn significant attention as promising materials for antimicrobial

applications regarding their versatile features. MOFs are organic-inorganic hybrid materials composed with metal ions or clusters and organic ligands, and have tunable porous structure with ultra-high surface area, allowing load of small molecules (Cai et al., 2021; Jiao et al., 2018). MOFs also have outstanding flexibility owing to their wide variety of metal ions/clusters and organic ligand materials.

ZIF-8, which is one of the most studied MOF, has a zeolitic topology with a large pore volume and surface area. It is known for its high thermal and chemical stability compared to zeolite or other MOFs (Park et al., 2006; Phan et al., 2010). Simple synthesis procedure and flexibility allows various modification, endowing great potentials to ZIF-8. Previous studies have confirmed that ZIF-8 has its own microbicidal activity (Du et al., 2021; Taheri et al., 2021). Also, modification of ZIF-8 was performed in a wide range to enhance the disinfection efficiency of ZIF-8 (Guo et al., 2018; Kohsari et al., 2016; Redfern et al., 2018; Wang et al., 2016).

Even though there has been extensive research about customizing ZIF-8, most studies only focused on the antimicrobial efficiency itself, not on the detailed reason of the microbicidal effect. Specifically, the antibacterial mechanism of ZIF-8 is still not clear, interrupting a thorough understanding of the underlying chemistry of ZIF-8. The precursors of ZIF-8, zinc ion and 2-methylimidazole (2-mim) were reported to be responsible for the inactivation due to their own toxicity (Abednejad et al., 2019; Taheri et al., 2021; Wang et al., 2016; Xu et al., 2020), but solid supporting evidence is lacking. In addition, other studies suggest that those precursors are not the main factors of the bactericidal activity (Li et al., 2019; Wang et al., 2021). Most studies have failed to identify mechanism in detail, and previous explanations conflict with each other, which is why the antibacterial mechanism of ZIF-8 needs

to be revisited.

Meanwhile, photocatalytic bactericidal activity of ZIF-8 was reported in 2019 (Li et al., 2019), which opened up new possibilities for ZIF-8 applications. In contrary to previous reports which mostly reported the band gap energy of ZIF-8 to be about 5 eV (Jing et al., 2014; Ren et al., 2019; Saliba et al., 2018; Yang et al., 2018), this paper insisted the band gap energy of ZIF-8 as 3.3 eV. According to the paper, reactive oxygen species (ROS) such as hydrogen peroxide (H_2O_2) and superoxide radical anion($O_2^{\cdot-}$) are generated with ZIF-8 under simulated solar irradiation. Although the wavelength range activating ZIF-8 is still controversial, photocatalytic activity of ZIF-8 has been demonstrated by past works. These recent findings, however, do not include the activity of ZIF-8 under visible light condition, which is remained as the research gap of the studies. Visible light accounts for about 44 % of solar light, whereas UV light only takes < 5% of solar light (Liebel et al., 2012; Moon et al., 2003). If ZIF-8 can utilize visible light sources for its photoactivation, the potent efficiency of ZIF-8 will be increased, which will lead to a wider range of the application field.

Herein, this work presents photo-enhanced bactericidal activity of ZIF-8 under visible light irradiation. Significant increase in antibacterial efficiency of ZIF-8 was observed with four different bacteria. In addition, by reexamining previous studies, disinfection mechanism of ZIF-8 was elucidated, which is not well known in the past. This paper revealed the synergistic disinfection effect which can be generated by the interaction between ZIF-8 precursors and bacterial component, eventually forming new complexation. UV-Vis DRS suggested that the Zn-mim-bacteria complex may be responsible for the visible light-activated bactericidal efficiency. The application

and usage of ZIF-8 can be extended upon their way based on comprehensive understanding of the bactericidal action of ZIF-8. This work provides valuable insights to future studies related to MOF in biological system by presenting the basic chemistry of ZIF-8 in disinfection area.

2. Materials & Methods

2.1. Reagents

All chemicals were reagent grade and used without further purification. Agar, nutrient broth (NB), tryptic soy broth (TSB), and tryptic soy agar (TSA) were purchased from Becton Dickinson. Zinc nitrate hexahydrate ($Zn(NO_3)_2 \cdot 6H_2O$), 2-methylimidazole (2-mim), isopropyl alcohol (IPA), methanol (MeOH), sodium chloride (NaCl), tert-butanol (t-BuOH), 4-hydroxy-TEMPO (TEMPOL), sodium azide (NaN_3), sodium oxalate ($Na_2C_2O_4$), sodium dichromate ($Na_2Cr_2O_7$), reduced l-glutathione (GSH), catalase from bovine liver, 4% osmium tetroxide solution, 25% glutaraldehyde solution, hexamethyldisilazane (HMDS), L-histidine, L-cysteine, 5,5-dimethyl-1-pyrroline N-oxide (DMPO), p-hydroxyphenylacetic acid (HPA), and horseradish peroxidase were purchased from Sigma-Aldrich. 3′-p-hydroxyphenyl fluorescein (HPF), and dihydroethidium (DE) were purchased from Invitrogen. Deionized (DI) water (18.2 MΩ cm, Milli-Q Integral Water Purification System, Millipore) was used for preparing solutions.

2.2. Synthesis and characterization of ZIF-8

ZIF-8 crystal was synthesized by simple procedure in MeOH solution (Sun et al., 2020). Briefly, 2.975 g of zinc nitrate hexahydrate and 3.08 g of 2-methylimidazole were dissolved respectively in 75 mL MeOH. 2-mim solution was added dropwise into zinc nitrate solution under stirring, and the mixture was stirred at room temperature for 24 h. Synthesized product was separated by centrifugation at 4000 rpm for 15 min and washed three times with MeOH. Final product was

obtained after drying in an oven for 12 h.

Scanning electron microscopy-energy dispersive spectroscopy (SEM-EDS) analysis and transmission electron microscopy (TEM) imaging was performed to observe the crystal structure (JSM-7800F Prime for SEM/JEM-3010 for TEM, JEOL), define atomic ratio and distribution of synthesized ZIF-8. The crystallinity of ZIF-8 was further determined by XRD patterns using X-ray diffractometer (Smartlab, Rigaku).

2.3. Culture and analysis of microorganisms

Four strains of bacteria were selected as surrogate microorganisms for inactivation experiment. Specifically, *S. aureus* (ATCC 25923), *B. subtilis* (ATCC 6633) were used as representatives of gram-positive bacteria, and *E. coli* (ATCC 8739), *P. aeruginosa* (ATCC 700829) were used as representatives of gram-negative bacteria. Bacteria cells were inoculated in 30 mL of medium (TSB for *S. aureus*, *B. subtilis*, and *P. aeruginosa*, NB for *E. coli*) and incubated at 37 °C for 18-24 h. The bacteria cells were collected by centrifugation at 3000 g for 15 min, and washed 3 times with 0.9 % NaCl solution. The obtained cells were resuspended in 20 mL of NaCl solution and kept at 4 ℃ until use. The spread plate method was used to determine the bacteria cell population. TSA plates were used for *S. aureus*, *B. subtilis*, *P. aeruginosa*, and nutrient agar plates were used for *E. coli*. The plates were incubated at 37 °C for 18-24 h before counting cell colonies.

2.4. Photocatalytic experiments

All experiments were conducted using 20 mL quartz reactors at room

temperature. Photocatalytic activity of ZIF-8 was evaluated under 300 W Xenon lamp (LS 150, Abet Technologies) with a UV cut-off filter (400 nm). Reaction was initiated by adding 10 mg of ZIF-8 into 20 mL bacterial solution (~ 10^8 CFU/mL) under vigorous stirring. 1 mL aliquot was carefully pipetted out at a predetermined interval. Sample was consequently diluted with saline solution and the bacterial concentration in the aliquot was determined by the spread plate method. The final pH of the photocatalytic experiments was all measured and maintained a slightly basic condition.

For reactive oxidant scavenging test, different scavengers were employed to quench the individual reactive species. Specific scavengers used in this study were IPA, MeOH, t-BuOH for hydroxyl radical (·OH), TEMPOL for superoxide radical anion ($O_2^{\cdot-}$), catalase for hydrogen peroxide (H_2O_2), NaN_3 for singlet oxygen ($^1O_2$), $Na_2C_2O_4$ for hole (h^+), $Na_2Cr_2O_7$ for electron (e^-), GSH for nonspecific antioxidant, and N_2 purging for anoxic condition. The concentration of each scavengers was adjusted for their maximum scavenging effect, and it was confirmed by control test that the scavengers do not affect the inactivation efficiency.

2.5. Measurement of ROS

Fluorescent probe compounds were used to analyze specific ROS. Fluorescence intensity was measured by microplate reader (Infinite M200, Tecan, Switzerland). HPF was used for measuring highly reactive oxygen species (hROS). Final concentration of HPF was 5 μM, excitation wavelength was 460 nm, and emission wavelength was 515 nm. DE was selected to analyze $O_2^{\cdot-}$. Final concentration of DE was 125 μM, and selected wavelength was 510 nm for excitation and 610 nm for

emission.

HPA was used to measure H_2O_2 in the system (Chen et al., 2018). Briefly, 0.027 g of HPA and 0.01 g of horseradish peroxidase were added to 8.2 g/L potassium hydrogen phthalate buffer solution, and 50 μL of the solution was added to 2 mL aliquot. After 10 min reaction, 1 mL of NaOH was added to quench the reaction. Excitation wavelength was 315 nm, and emission wavelength range was 350-500 nm. HPF and DE were added simultaneously with the initiation of inactivation experiment to measure cumulative ROS. HPA was added into withdrawn aliquots to analyze steady-state H_2O_2.

2.6. Analytical methods

The concentration of 2-mim, phenol (PhOH), and furfuryl alcohol (FFA) was analyzed with ultrahigh performance liquid chromatography (UltiMate 3000, Thermo Fisher Scientific). Electron spin resonance (ESR) analysis was conducted with ESR spectrometer (JES-X310, JEOL). UV-Vis spectrum of the complex was monitored by UV-Vis spectrometer (Lambda 465, PerkinElmer). Mass spectrum data was acquired by mass spectrometry (TSQ Quantum Discovery MAX, Thermo Fisher Scientific). UV-Vis diffuse reflectance spectra (DRS) was obtained by UV-Vis-NIR spectrophotometer (UV-3600i Plus, SHIMADZU). Bacterial samples for SEM analysis were prepared by following the steps described elsewhere (Mogana Das and Patchamuthu, 2016).

3. Results and Discussion

3.1. ZIF-8 characterization

Crystalline shape of ZIF-8 was observed using SEM and TEM image. ZIF-8 was well synthesized to rhombic dodecahedron crystal (Fig. 1a and Fig. 1b), which is the most thermally stable structure among possible structure of ZIF-8 (Troyano et al., 2019). The synthesized ZIF-8 had an average crystal size of 1 μm. XRD patterns also confirmed the typical sodalite structure of ZIF-8 (Fig. 1c). The synthesized ZIF-8 exhibited characteristic peaks at 2θ=7.30°, 10.35°, 12.70°, 14.80°, 16.40°, and 18.00° corresponding to (110), (200), (211), (220), (310), and (222) planes (Ahmad et al., 2021). The crystallinity of ZIF-8 maintained high stability under visible light irradiation. Atomic distribution and composition of ZIF-8 was determined by EDS analysis. EDS analysis indicated that the elements were well distributed (Fig. 1d). The atomic ratio of each element was 64.18%, 27.17%, 7.04% for carbon, nitrogen, and zinc, respectively, which is consistent with the molecular atomic ratio of ZIF-8 (Fig. 1e).

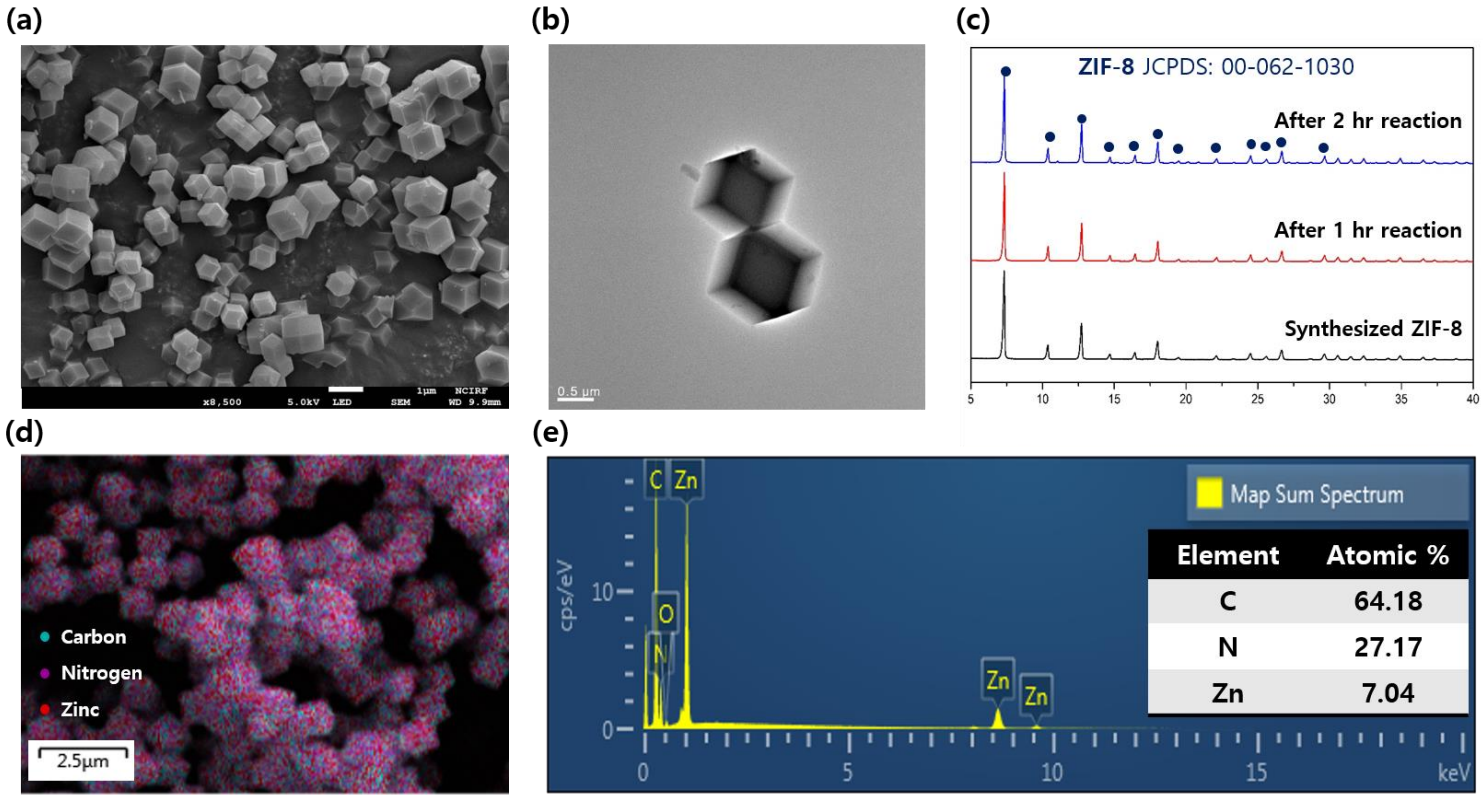

Figure 1. (a) SEM image, (b) TEM image, (c) XRD patterns, (d), (e) EDS analysis of the synthesized ZIF-8.

$[\text{ZIF-8}]_0$ = 0.5 g/L; Xenon lamp = 150 W (λ > 400 nm, 100 mW/cm^2);

3.2. Bacterial inactivation by ZIF-8

The inactivation of four representative bacteria was examined after the treatment with ZIF-8. The bactericidal activity of ZIF-8 was first observed under dark condition. Without light, 1.5 log inactivation in 60 min was achieved for *E. coli* (Fig. 2a), 1.3 log inactivation for *P. aeruginosa* and 0.9 log inactivation for *B. subtilis* (Fig. 2b). *S. aureus* was not strongly affected by ZIF-8 inactivation under dark condition.

The bactericidal activity of ZIF-8 was enhanced by visible light illumination, and such enhancement was observed for the different bacterial species. *E. coli*, *P. aeruginosa*, *S. aureus*, and *B. subtilis* were inactivated by 3.7 log, 3.8 log, 2.2 log, and 2.1 log, respectively. The degree of increased antibacterial activity was greater in gram-negative bacteria than in gram-positive bacteria. This result can be explained by different outer cell wall structure of bacteria. Gram-positive bacteria possess 20-80 nm thickness of peptidoglycan cell wall, which is relatively thick compared to that of gram-negative bacteria (1.5 – 10 nm). Since gram-negative species have thinner cell wall, those species are more vulnerable to the antibacterial system and thus can be inactivated significantly (Mai-Prochnow et al., 2016).

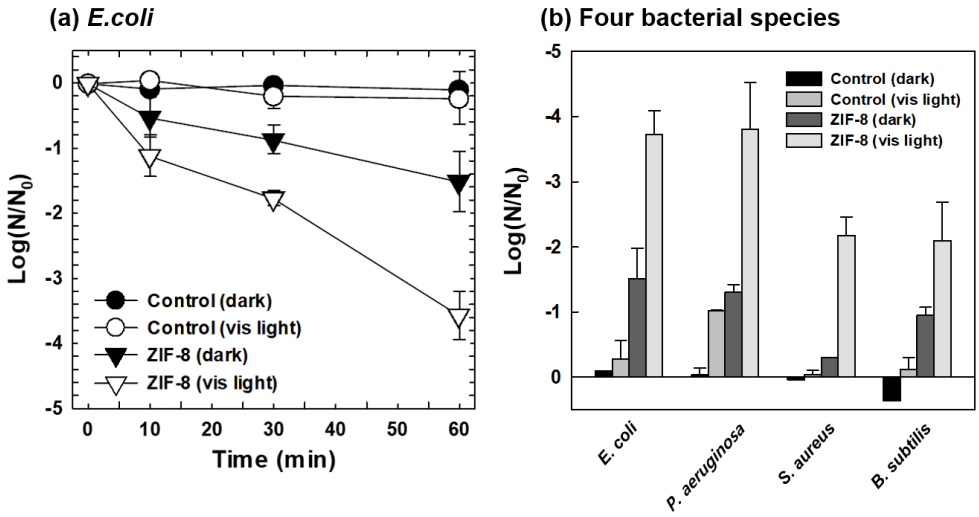

Figure 2. (a) Inactivation of *E. coli* by ZIF-8, (b) Inactivation efficiency of ZIF-8 under visible light irradiation.

$[\text{ZIF-8}]_0$ = 0.5 g/L; $[E.\ coli]_0$, $[P.\ aeruginosa]_0$, $[S.\ aureus]_0$, $[B.\ subtilis]_0$ = N×10^7 CFU/mL; Xenon lamp = 150 W (λ > 400 nm, 100 mW/cm^2);

Morphological changes of bacterial cells were observed by SEM analysis. SEM images of the bacterial cells demonstrate that ZIF-8 ruptured cell membrane effectively (Fig. 3). While intact bacterial cells maintained their original shape and volume (Fig. 3a and Fig. 3d), inactivated bacterial cells undergone cell distortion and shrinkage. The morphology of *E. coli* and *S. aureus* were totally destructed in presence of ZIF-8 with visible light illumination, suggesting extensive physical damage on bacterial cell membranes (Fig. 3c and Fig. 3f) (Lee et al., 2009). Without light, only *E. coli* suffered cell destruction (Fig. 3b and Fig. 3e), which is agreeable with the inactivation data.

Bacterial cell damage was further monitored by fluorescent microscopy with *Bac*light LIVE/DEAD cell staining. Healthy bacterial cells used as control were stained green because membrane damage was not induced (Fig. 4). Most of *E. coli* cells treated with ZIF-8 under visible light irradiation were stained red, indicating cell death due to the disruption of cell membrane integrity.

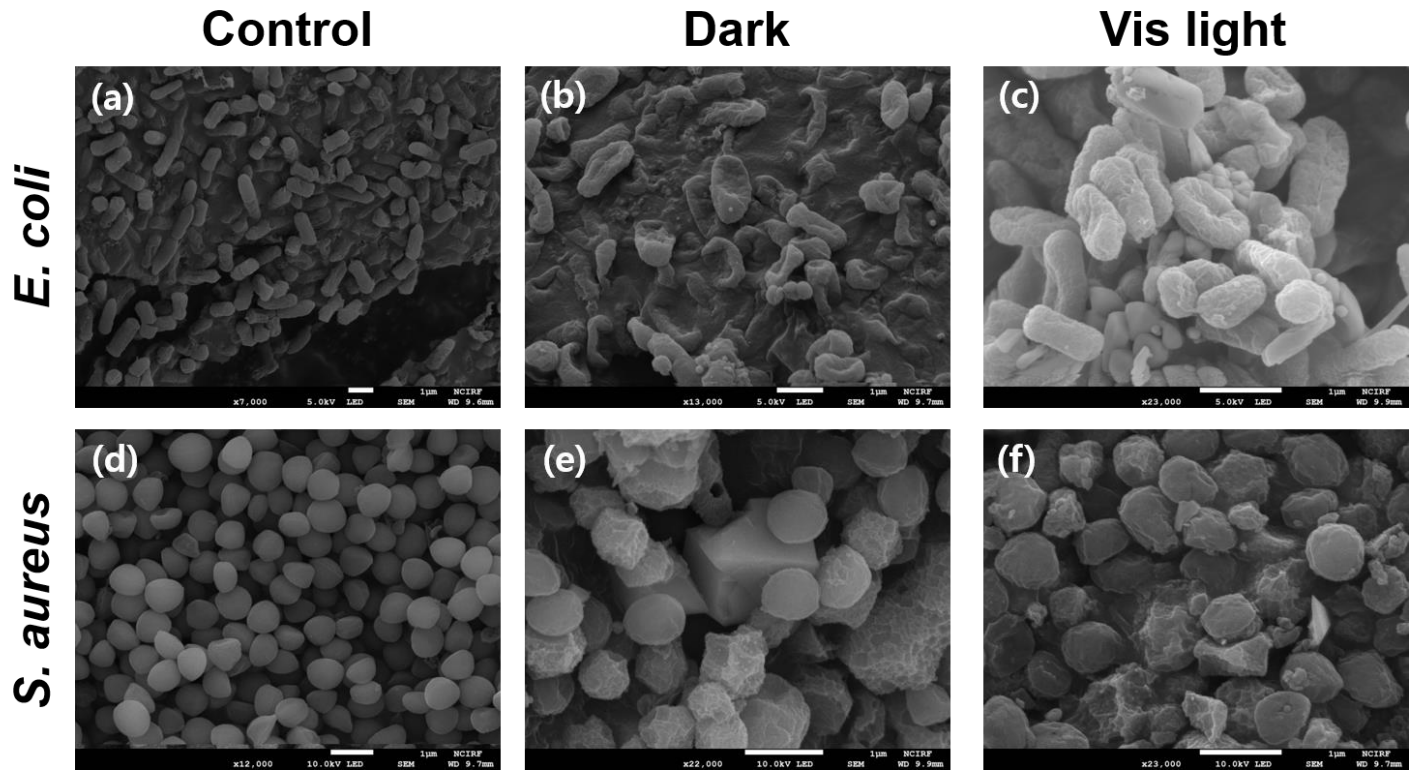

Figure 3. SEM images of *E. coli* and *S. aureus* treated by ZIF-8.

$[\text{ZIF-8}]_0$ = 0.5 g/L; $[E.\ coli]_0$, $[S.\ aureus]_0$ = N×10^7 CFU/mL; Xenon lamp = 150 W (λ > 400 nm, 100 mW/cm^2);

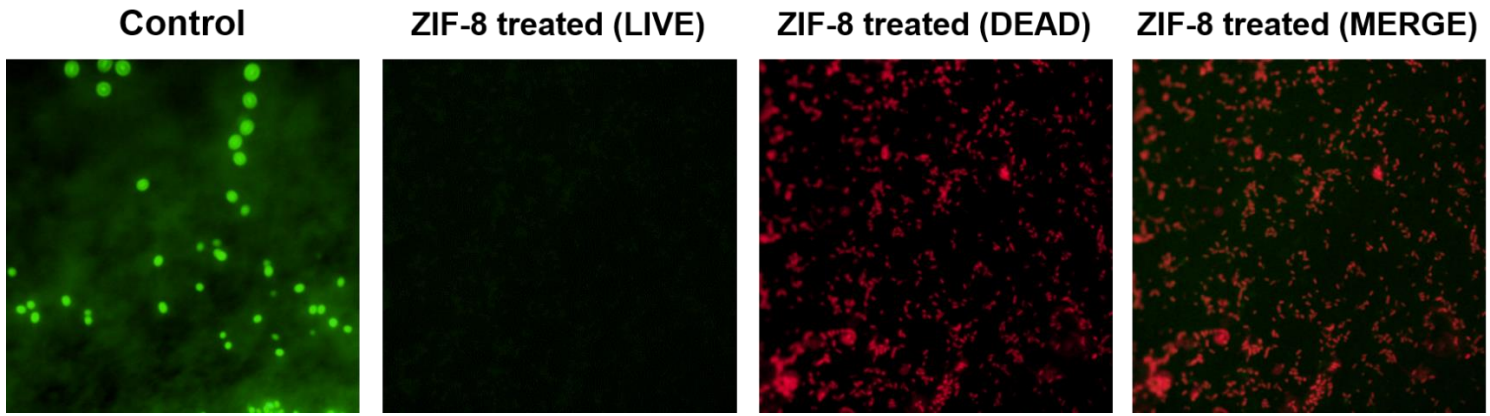

Figure 4. *Bac*light LIVE/DEAD cell staining of *E. coli*.

$[\text{ZIF-8}]_0$ = 0.5 g/L; $[\textit{E. coli}]_0$ = N×10^7 CFU/mL; Xenon lamp = 150 W (λ > 400 nm, 100 mW/cm^2);

3.3. Antibacterial mechanism of ZIF-8

3.3.1. ROS measurement

To investigate ROS generation caused by ZIF-8, ESR technique was applied to monitor the reactive oxidants produced in the system. DMPO was selected as a free-radical spin trapping agent. In aqueous condition, there was no identifiable spin adduct peak, indicating no ·OH generation. DMSO, an aprotic solvent, was introduced into the system to stabilize the DMPO-OOH adduct, allowing the observation of $O_2^{\cdot -}$ generation (Diaz-Uribe et al., 2010; Finkelstein et al., 1982). As a result, DMPO-OOH peaks were appeared in presence of ZIF-8 irradiated with visible light in DMSO solution (Fig. 5a). The intensity of DMPO-OOH peaks was increased continuously over time. DMPO-X peaks were also observed, indicating the oxidation of DMPO. DMPO-OH peak, which can be generated by ·OH, was not observed in both solutions.

ROS scavenging test was conducted to evaluate the attribution of specific reactive oxidants. Different scavengers were employed to quench the specific ROS and the bacterial inactivation rates were measured with each reagent. The addition of scavengers inhibited the *E. coli* inactivation to different extents, except for IPA, which is known as ·OH scavenger (Fig. 5b). Inactivation efficiency was decreased by 80% with TEMPOL ($O_2^{\cdot -}$ scavenger), 86% with catalase (H_2O_2 scavenger), 49% with NaN_3 ($^1O_2$ scavenger), 80% with $Na_2C_2O_4$ (h^+ scavenger), 76% with $Na_2Cr_2O_7$ (e^- scavenger), 83% with GSH (nonspecific antioxidant), and 96% with N_2 purging (anoxic condition). Among various scavengers, N_2 purging for anoxic condition was mostly effective to hinder the inactivation activity of ZIF-8, indicating that oxygen

plays an important role in the oxidative bactericidal activity of ZIF-8.

Further experiments with different alcohols used as ·OH scavenger and ESR analysis confirmed that ·OH is not available in the solution. Interestingly, total elimination of the bactericidal activity of ZIF-8 by t-BuOH was observed. Bulky t-BuOH may interfere the possible interaction between ZIF-8 surface or precursors and bacterial components, hindering the bactericidal reaction by surface-bound ROS and other surface sites (Kim and Choi, 2002; Minero et al., 2000; Nosaka and Nosaka, 2017). To obtain more information of produced ROS, organic compound degradation using ZIF-8 was monitored by HPLC analysis (Fig. 6). However, PhOH and FFA oxidation was negligible in 60 min under visible light irradiation. This result shows that the amount of generated ROS in this system is not sufficient for chemical degradation.

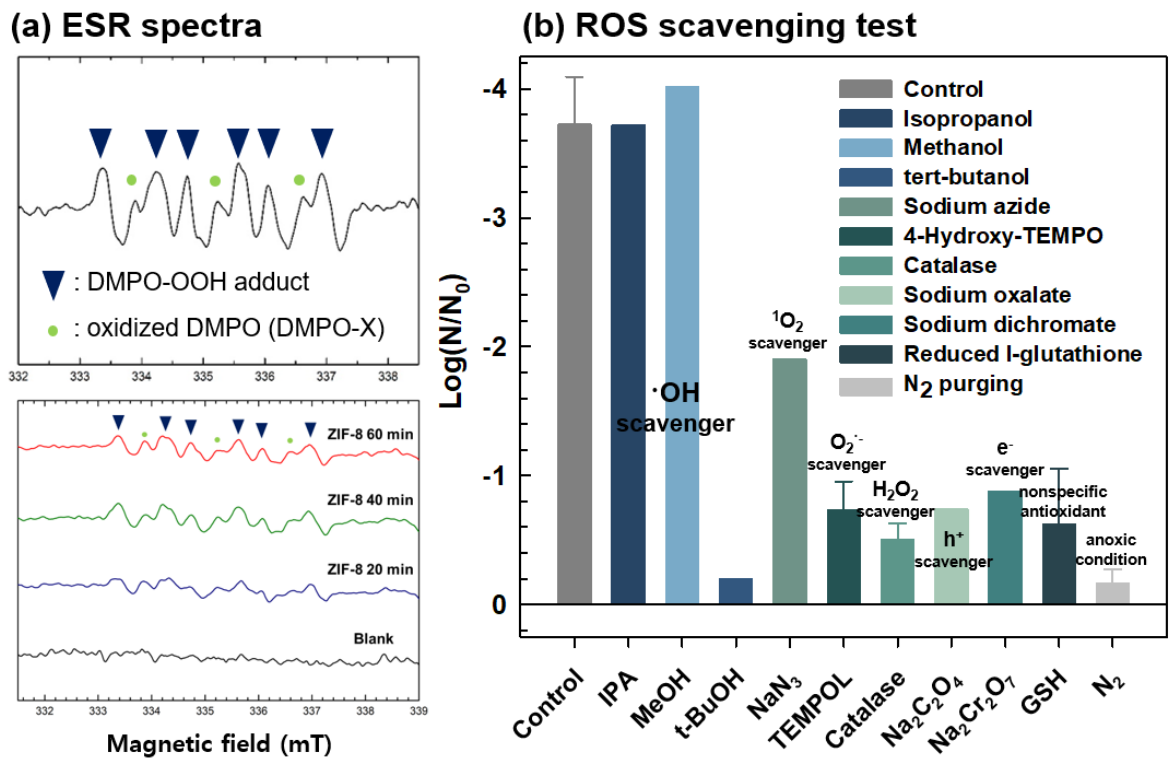

Figure 5. (a) ESR spectra of ZIF-8 using 5,5-dimethyl-1-pyrolline-N-oxide and (b) ROS scavenger test under visible light irradiation. (a) $[\text{ZIF-8}]_0$ = 1 g/L; [DMPO] = 10 mM; Power = 5 mW; Amplitude = 800 (top), 200 (bottom); $[\textit{E. coli}]_0 = N \times 10^8$ CFU/mL; Xenon lamp = 150 W (λ > 400 nm, 200 mW/cm^2); (b) $[\text{ZIF-8}]_0$ = 0.5 g/L; $[\textit{E. coli}]_0 = N \times 10^7$ CFU/mL; Xenon lamp = 150 W (λ > 400 nm, 100 mW/cm^2);

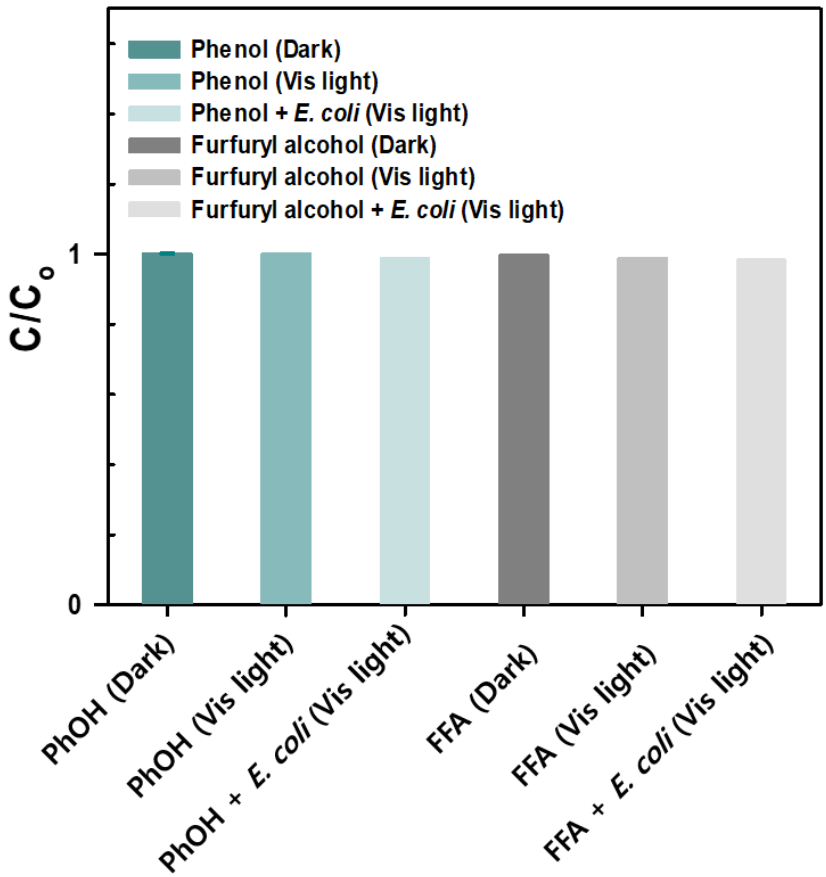

Figure 6. Phenol and furfuryl alcohol degradation using ZIF-8 and bacteria. $[PhOH]_0$, $[FFA]_0$ = 50 uM; $[ZIF\text{-}8]_0$ = 1 g/L; $[E.\ coli]_0 = N \times 10^8$ CFU/mL; Xenon lamp = 150 W ($\lambda > 400$ nm, 100 mW/cm^2); All samples were filtered before analysis.

Individual ROS generation was measured using fluorescent probes, which have great sensitivity to detect the low quantity of ROS. HPF and DE were selected to measure cumulative hROS and $O_2^{\cdot-}$, respectively. Presence of the bacterial cells remarkably enhanced the relative fluorescent intensity in the system (Fig. 7a and Fig. 7b), implying that ROS generation is mainly affected by accompanying bacterial cell components. hROS are suggested as ROS which are strong enough to proceed the *ipso*-substitution reaction of HPF probe (Setsukinai et al., 2003), and mostly indicates ·OH. However, it is proved by other experiments that ·OH is unlikely to be formed in this system. Therefore, hROS detected by HPF in this system would be reactive intermediates generated by bacterial cell component (Urano et al., 1996), supported by the result that ZIF-8 without bacterial cells did not exhibit any difference between visible light and dark condition. ·OH scavenging by IPA did not influence the fluorescence intensity, which is consistent with other data.

The concentration of steady-state H_2O_2, on the other hand, was lower in presence of bacterial cell (Fig. 7c). This result can be explained by the difference from the analytical methods. HPA was employed to measure the steady-state H_2O_2. H_2O_2 can be freely generated and consumed in the system, so only residual H_2O_2 will be detected by HPA after the interval sampling. Since ROS in the system can be easily consumed by the bacterial cells, it is no surprise that the amount of steady-state H_2O_2 decreased in presence of the bacterial cells. hROS and $O_2^{\cdot-}$ were generated and detected in a real time without further consumption because the probes were added simultaneously with the initiation of reaction. The results altogether suggest that the presence of bacterial cells in ZIF-8 system generates and consumes more ROS under visible light irradiation, influencing the bactericidal effect.

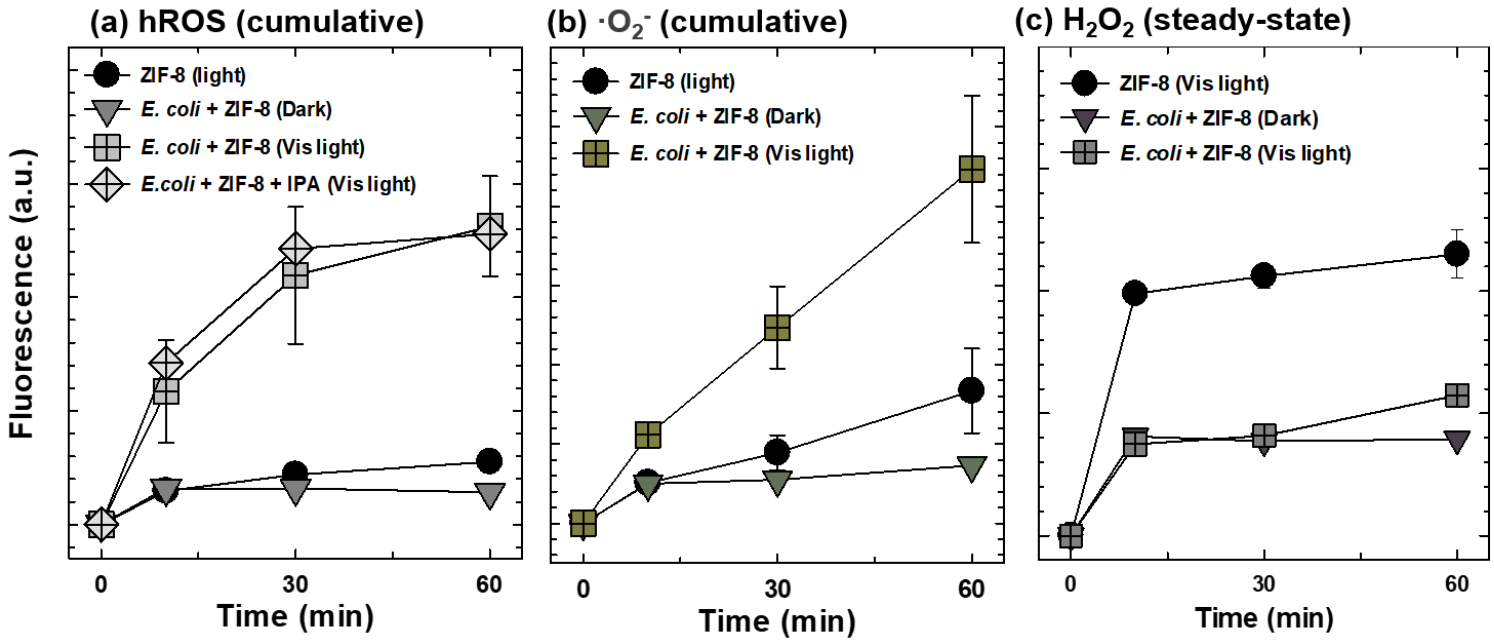

Figure 7. ROS detection by ZIF-8 under visible light irradiation (a) hROS accumulation using HPF. [HPF] = 5 μM; λext = 460 nm; λems = 515 nm; (b) O_2^{-} accumulation using DE. [DE] = 125 μM; λext = 510 nm; λems = 610 nm; (c) H_2O_2 detection using HPA. [p-HPA] = 0.291 μM; λ_{Ext} = 315 nm; λ_{Ems} = 350-500 nm; $[ZIF\text{-}8]_0$ = 1 g/L; $[E.\ coli]_0 = N \times 10^8$ CFU/mL; Xenon lamp = 150 W (λ > 400 nm, 100 mW/cm^2); All samples were filtered before analysis.

3.3.2. The effect of ZIF-8 precursors

Although oxygen seems to have correlation with the bacterial disinfection, the amount of produced ROS was too small to be certain that ROS are the primary causes of antibacterial activity of ZIF-8. Another possible explanation for the bactericidal action of ZIF-8 was discussed in past studies that zinc ion and 2-mim, which are the precursors of ZIF-8, are both responsible for inactivation efficiency. Each component is known for its own cytotoxicity; the disinfection ability of zinc-based materials is generally described by the release of zinc ions (Franklin et al., 2007; Li et al., 2011; Rani et al., 2013), and 2-mim is considered to have antimicrobial activity by destroying phospholipid structure with unsaturated fatty acids (Bahnous et al., 2013; Sud et al., 1979). Taken together with past studies, it can be thought that the visible light-enhanced activity of ZIF-8 can be explained by the increase in the amount of precursors released from ZIF-8, since photo-accelerated degradation of ZIF-8 has been reported (Taheri and Tsuzuki, 2021).

Contrary to the expectations, tracking the amount of released ZIF-8 precursors revealed that degradation of ZIF-8 is not accelerated under visible light irradiation, thus cannot be the reason for the photo-enhanced antibacterial activity (Fig. 8). Released precursors of ZIF-8 and decomposition percentage of ZIF-8 in aqueous solution were measured by UV-vis spectroscopy. 2-mim was selected as a tracking precursor since zinc ion exists as an insoluble form in basic condition (pH 8) with ZIF-8 (Reichle et al., 1975). There was no difference between two conditions until 60 min, and only slight difference was observed after 120 min. Calculated percentage of ZIF-8 decomposition was 12.5 % under visible light irradiation, and 11.7 % without light in 60 min. Filtrate of the solution after 60 min reaction was also

obtained to examine the effect of released ions. However, the filtrate did not show any bactericidal activity (Fig. 9). Plus, no significant pH change was observed to destroy bacterial environment (Fig. 10).

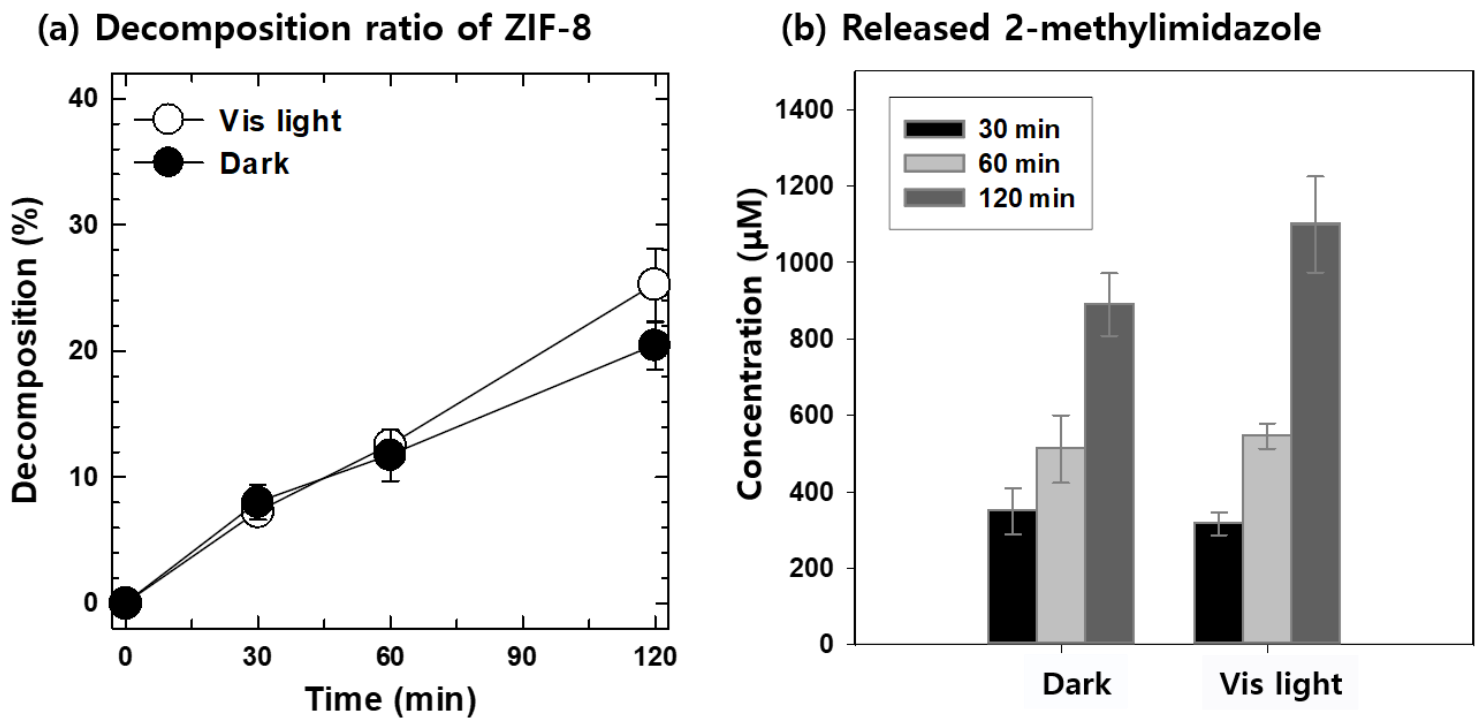

Figure 8. (a) Decomposition wt % of ZIF-8 in aqueous soluttion with and without the illumination, (b) Measured 2-mim by UV-vis absorption spectroscopy.

$[ZIF\text{-}8]_0$ = 0.5 g/L; Xenon lamp = 150 W (λ > 400 nm, 100 mW/cm^2);

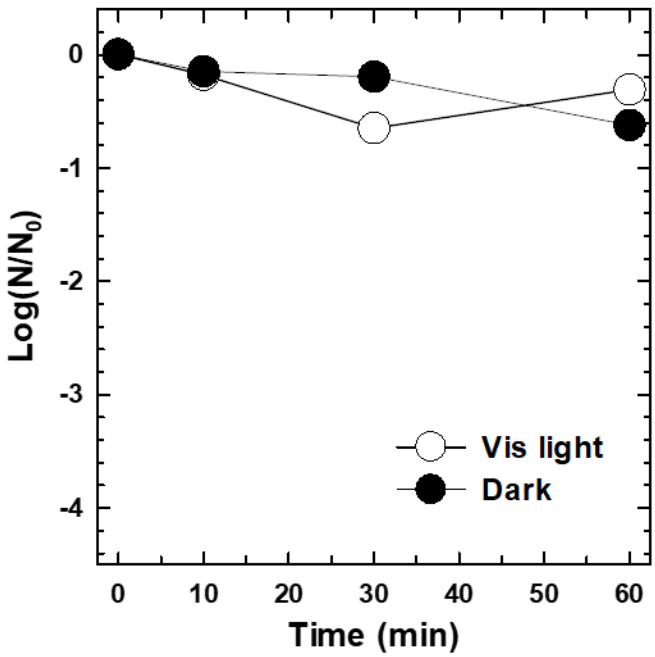

Figure 9. Disinfection performance of the filtrate of ZIF-8 after 60 min reaction under visible light.

[*E. coli*]$_0$ = N×10^7 CFU/mL; [ZIF-8]$_0$ = 0.5 g/L; Xenon lamp = 150 W (λ > 400 nm, 100 mW/cm^2);

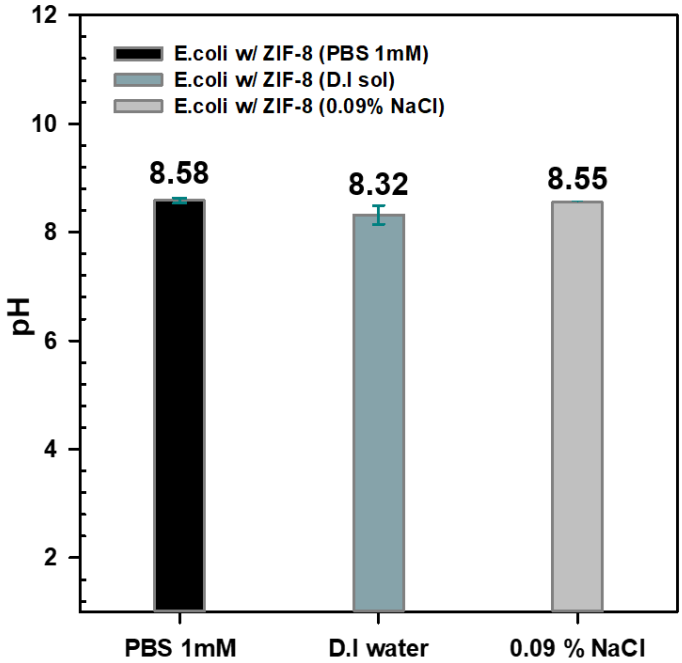

Figure 10. Final pH of ZIF-8 solution after 60 min reaction.

$[E.\ coli]_0$ = N×10^7 CFU/mL; $[ZIF\text{-}8]_0$ = 0.5 g/L; Xenon lamp = 150 W (λ > 400 nm, 100 mW/cm^2);

Zinc ion or 2-mim alone did not result in significant *E. coli* inactivation under visible light condition (Fig. 11), which was an unexpected result from past studies. To evaluate the bactericidal activity of each precursors of ZIF-8, excessive amount of zinc ion and 2-mim was added into the bacterial solution respectively. The concentration of the precursors was three times higher than the original experimental concentration of ZIF-8. Disinfection of *E. coli* was not observed even with large amount of zinc ion or 2-mim, indicating that the bactericidal activity of ZIF-8 cannot simply be explained by the sum of the activities of zinc ion and 2-mim.

Interestingly, when zinc and 2-mim were added simultaneously as same as the concentration of ZIF-8, they exhibited similar activity to ZIF-8. This result suggests that zinc ion with 2-mim shows the synergistic antibacterial effects only when they coexist. Therefore, the interaction between zinc ion and 2-mim may be the key factor for the bactericidal activity of ZIF-8. To clarify the importance of the interaction between zinc ion and 2-mim, zinc binding agent such as phosphate ion or EDTA was introduced to this system. Phosphate ion and EDTA are both reported to undergo the complexation with zinc ion in aqueous solution (Taheri et al., 2021). As a result, this chelation of zinc successfully hindered the interaction of ZIF-8 precursors, eliminating visible light-activated antibacterial efficiency of ZIF-8.

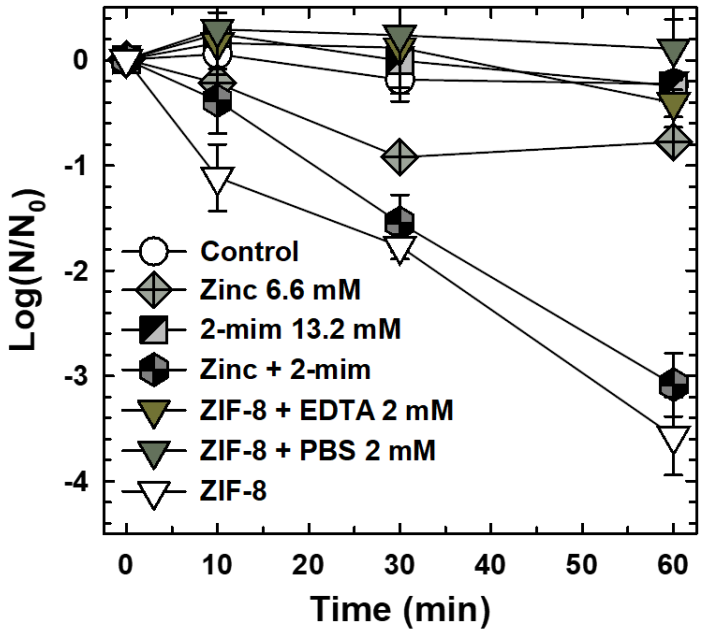

Figure 11. The inactivation efficiency of ZIF-8 precursors and the effect of zinc binding agent under visible light condition.

$[\text{ZIF-8}]_0$ = 0.5 g/L; $[\textit{E. coli}]_0$ = N×10^7 CFU/mL; Xenon lamp = 150 W (λ > 400 nm, 100 mW/cm^2);

3.3.3. Zn-mim-bacteria complex formation

Zinc ion in combination with 2-mim shows synergistic antibacterial effects under both dark and visible light conditions. Increased activity of the Zn(II)-mim complexes under dark condition can be partially explained by the overlap of the metal and ligand orbital (Fettouhi et al., 2007; Joseyphus and Nair, 2008; Wazeer et al., 2007). Previous studies suggest that this overlap increases lipophilicity of Zn(II)-mim complexes, thereby making it easier to penetrate into the bacterial cell membrane. The complexes that have penetrated into the cells may interact with substances inside, and cause a damage to the cellular components.

The absorbance spectra of Zn-mim-*E. coli* complex was monitored to detect the cellular interaction with precursors of ZIF-8. Zinc and 2-mim in the bacterial solution exhibited synergistic changes in UV-vis absorption spectra, indicating that the complexation of ZIF-8 with cellular components were occurred in the system (Fig. 12). To get more information about the interaction, time-dependent profile of free 2-mim available in the system was measured by HPLC analysis. Free 2-mim was less detected in aqueous solution with bacterial cells, since bacterial components can actively go through the reaction with free 2-mim (Fig. 13).

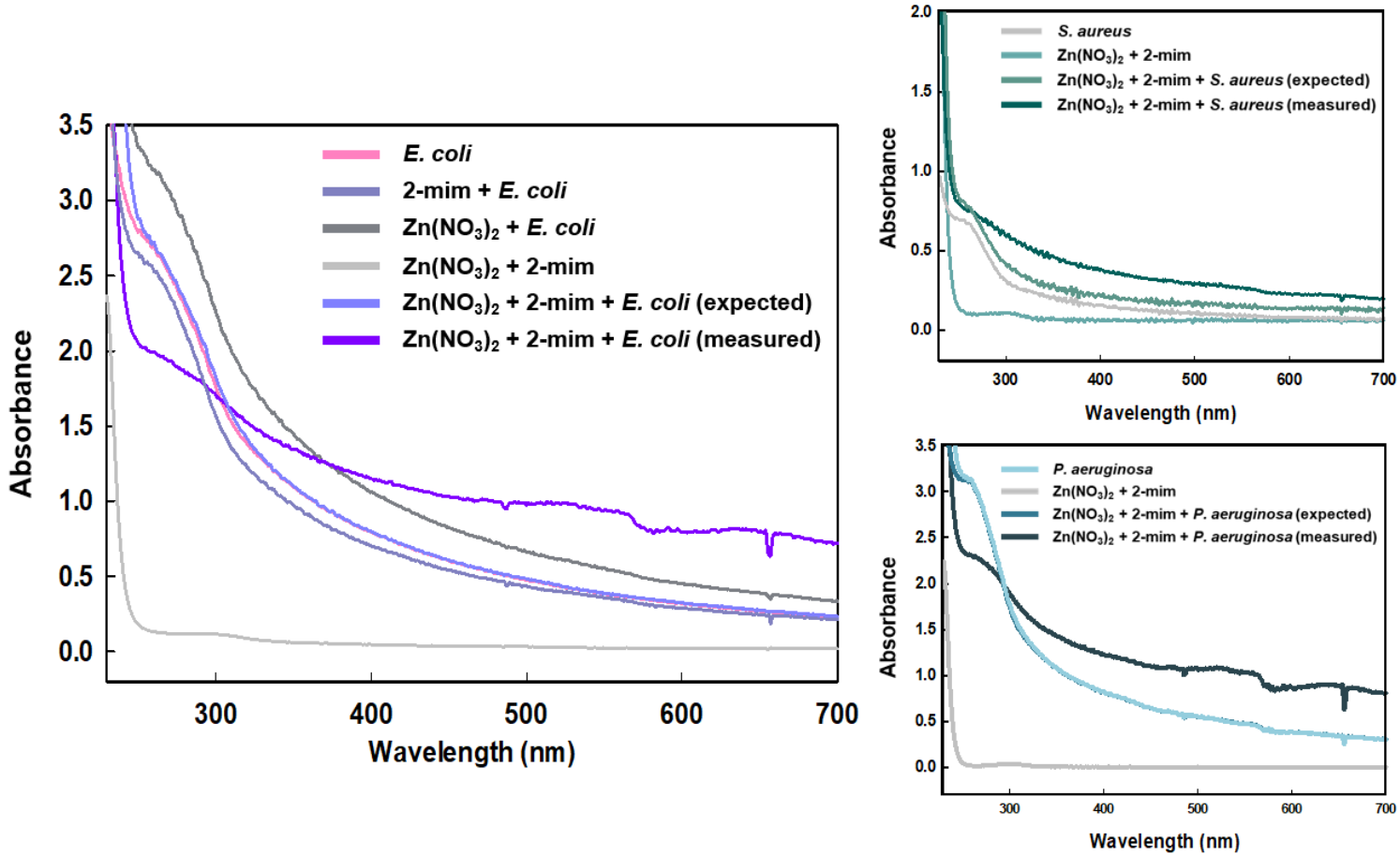

Figure 12. Absorbance data of ZIF-8 precursors and *E.coli* (left), *S. aureus* and *P. aeruginosa* (right).

$[\text{ZIF-8}]_0$ = 0.5 g/L; $[\text{Bacteria}]_0$ = N×10^7 CFU/mL; Xenon lamp = 150 W (λ > 400 nm, 100 mW/cm^2);

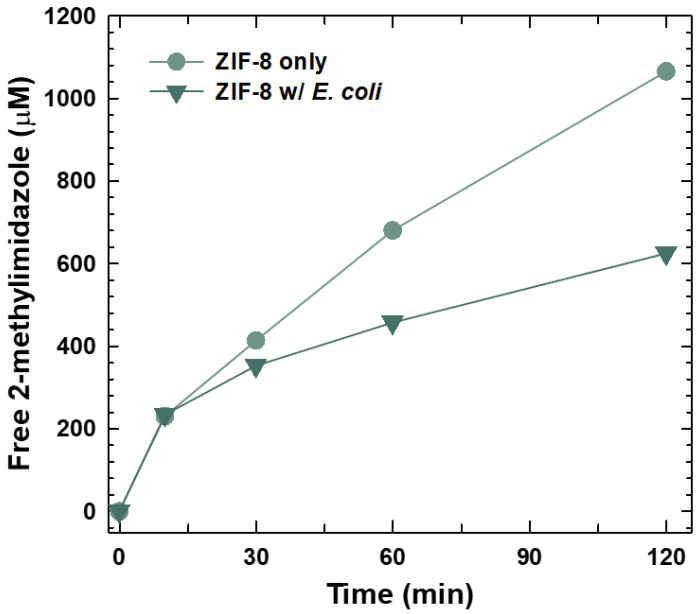

Figure 13. The amount of free 2-mim measured by HPLC with or without *E. coli*. $[\text{ZIF-8}]_0$ = 0.5 g/L; $[E.\ coli]_0$ = N×10^7 CFU/mL; Xenon lamp = 150 W (λ > 400 nm, 100 mW/cm^2);

The interactions between ZIF-8 (Zn-(2-mim)$_2$) and specific bacterial components were observed in molecular level using ESI-MS. Key amino acids such as histidine and cysteine were selected for the representative of the bacterial components because of their affinity with zinc ion and pH range in aqueous solution. When histidine was added to the system, histidine was gradually substituted for 2-mim (Fig. 14a, 14b). (2-mim)-Zn-His complex peak was slightly decreased in 60 min, while Zn-(His)$_2$ complex peak has increased over time. Cysteine exhibited different activity with histidine. Cysteine was gradually added to ZIF-8 structure, generating (2-mim)$_2$-Zn-Cys complex (Fig. 14c, 14d). Since all samples were filtered before analysis, insoluble complexes such as original ZIF-8 could not be detected. Overall, substitution and addition of amino acids to ZIF-8 were observed, suggesting the possibility of Zn-mim-bacteria complex formation during disinfection reaction of ZIF-8.

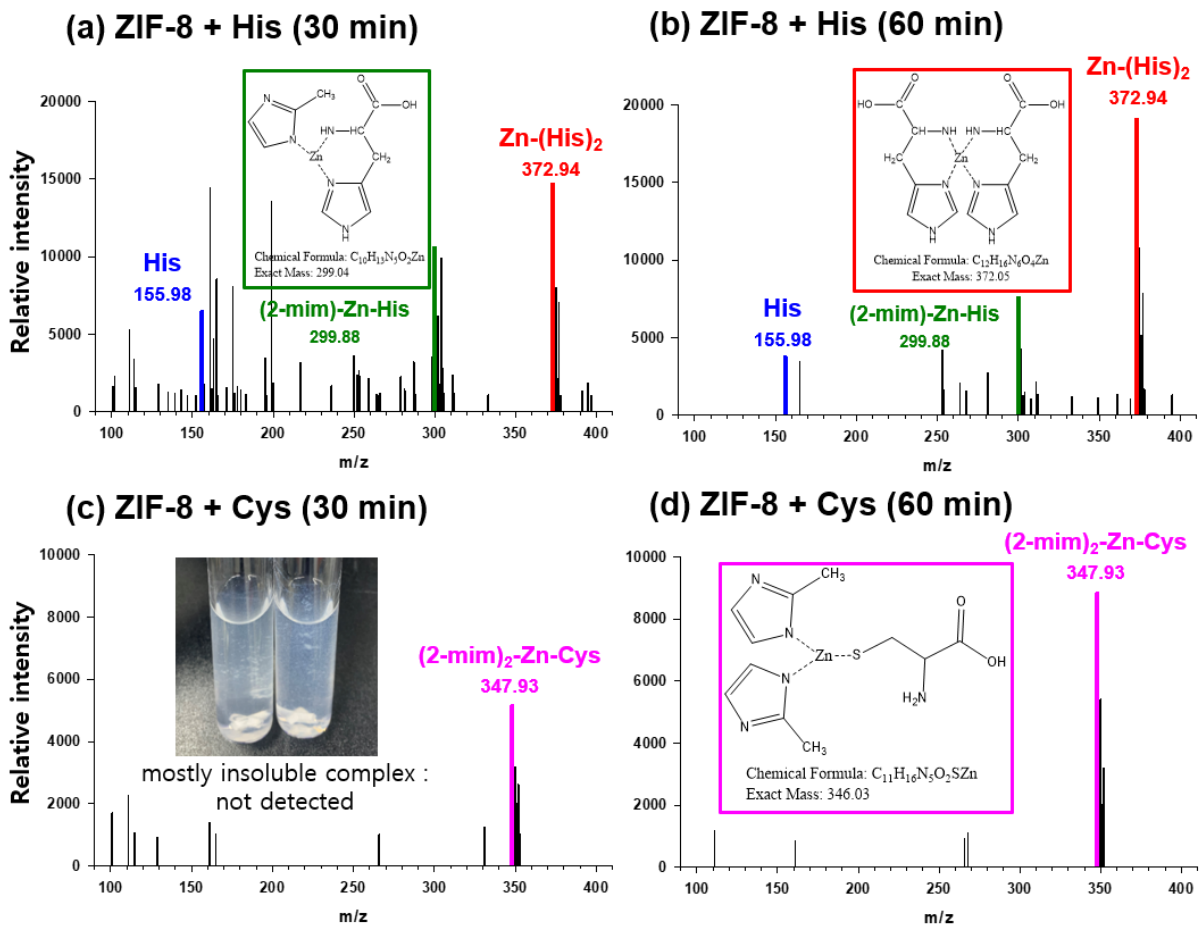

Figure 14. Mass spectrometry of reaction between ZIF-8 and histidine and cysteine.

$[\text{ZIF-8}]_0$ = 0.5 g/L; [Amino acid] = 2.2 mM; All samples were filtered before analysis.

To find out whether Zn-mim-bacteria complex formation influences the visible light-activation of ZIF-8, UV-vis diffuse reflectance spectroscopy was performed. Measured band gap energy of synthesized ZIF-8 was 5.1 eV (Fig. 15a), which is consistent with previous reports. *E. coli* had the band gap energy of 4.1 eV, and showed a little peak in NIR region. ZIF-8/bacterial complex exhibited three peaks in UV-Vis diffuse reflectance spectrum (Fig. 15b). Two peaks in UV region were assigned to be peaks from original ZIF-8 and *E. coli*. Final peak in the visible light region was newly generated by the complexation of ZIF-8 with *E. coli*, and the band gap was calculated to 2.76 eV. This new UV-vis spectrum peak was observed repeatedly with new bacterial ZIF-8 complex. It indicates that the Zn-mim-bacteria complex may be responsible for photo-activity in the visible light region, which was unexplainable by the large band gap of ZIF-8.

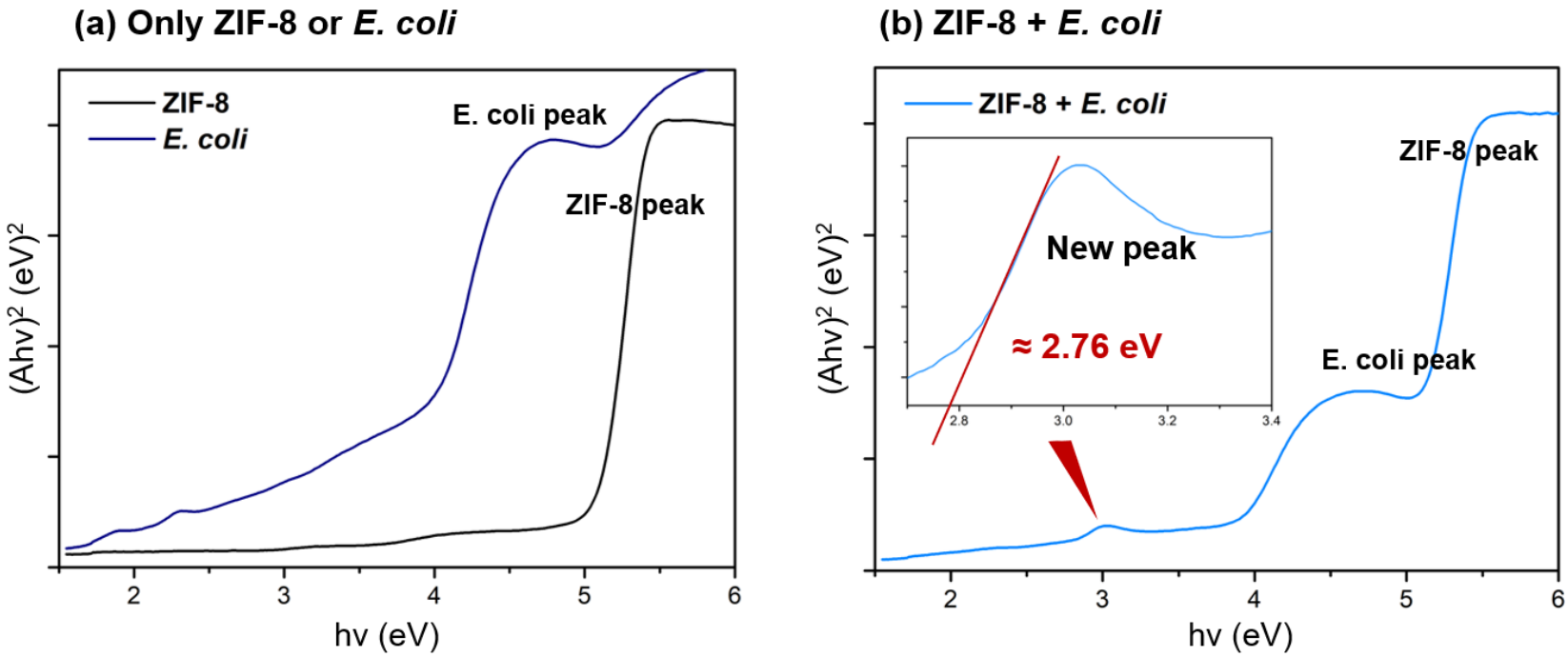

Figure 15. UV-Vis DRS analysis and calculated band gap of synthesized ZIF-8 and new complex. $[\text{ZIF-8}]_0$ = 1 g/L; $[\textit{E. coli}]_0 = 10^8$ CFU/mL; Xenon lamp = 150 W ($\lambda > 400$ nm, 100 mW/cm^2);

Based on the above results, the interaction between ZIF-8 precursors and bacterial cells are the primary cause of disinfection ability of ZIF-8. Moreover, Zn-mim-bacteria complex formed from the interaction may also be responsible for the visible light-enhanced bactericidal activity of ZIF-8. The overall scheme of photo-enhanced activity of Zn-mim-bacteria complex in the system is elaborated in Fig. 16.

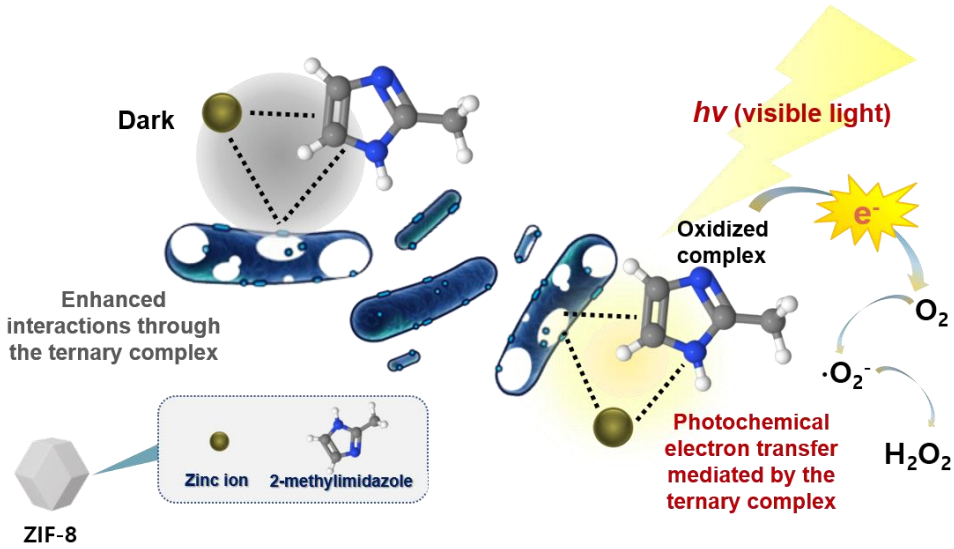

Figure 16. Schematic diagram of suggested disinfection mechanism

4. Conclusions

This study firstly demonstrated visible light-enhanced inactivation ability of ZIF-8, which is unexplainable with the large band gap of ZIF-8. ZIF-8 exhibited significantly increased disinfection activity toward different bacterial species under visible light irradiation. The inactivation experiment using ZIF-8 precursors and metal chelators declared the synergistic antibacterial effect of ZIF-8, denying the sole effect of ZIF-8 precursors suggested in previous works. UV-Vis spectra, HPLC, and mass spectrometry confirmed the formation of Zn-mim-bacteria complex in this system. Also, UV-vis DRS suggested that Zn-mim-bacteria may play a vital role for the photo-enhanced disinfection of ZIF-8. The photochemical reactions of the Zn-mim-bacteria complexes may be responsible for the enhanced inactivation of *E. coli* by visible light-illuminated ZIF-8; the electron transfer from the cell to oxygen can be mediated through the ternary complex. ESR analysis, ROS scavenger test, and fluorescent assay showed that ROS ($O_2^{\cdot -}$, H_2O_2 and biological intermediates) form during the *E. coli* inactivation by illuminated ZIF-8, although their contribution to the bacterial inactivation has to be further clarified.

This comprehensive understanding of ZIF-8 precursors and biological system indicates that the activity of MOF cannot be interpreted simply by the characteristics of MOF, and has to consider the influence of surrounding environment. The findings in this work will provide the basic understanding about ZIF-8 in biological system, which can encourage significant achievements in environmental and biomedical applications using ZIF-8.

References

Abednejad, A., Ghaee, A., Nourmohammadi, J., Mehrizi, A. A., 2019. Hyaluronic acid/ carboxylated Zeolitic Imidazolate Framework film with improved mechanical and antibacterial properties. Carbohydr. Polym. 222, 115033.

Ahmad, N., Nordin, N. A. H. M., Jaafar, J., Ismail, A. F., Ramli, M. K. N. B., 2021. Significant improvement in antibacterial property of ZIF-8 decorated graphene oxide by post-synthetic modification process. J. Environ. Chem. Eng. 9(5), 105887.

Bahnous, M., Bouraiou, A., Chelghoum, M., Bouacida, S., Roisnel, T., Smati, F., Bentchouala, C., Gros, P. C., Belfaitah, A., 2013. Synthesis, crystal structure and antibacterial activity of new highly functionalized ionic compounds based on the imidazole nucleus. Bioorg. Med. Chem. Lett. 23(5), 1274-1278.

Cai, G., Yan, P., Zhang, L., Zhou, H.-C., Jiang, H.-L., 2021. Metal–Organic Framework-Based Hierarchically Porous Materials: Synthesis and Applications. Chem. Rev. 121(20), 12278-12326.

Chen, N., Shang, H., Tao, S., Wang, X., Zhan, G., Li, H., Ai, Z., Yang, J., Zhang, L., 2018. Visible Light Driven Organic Pollutants Degradation with Hydrothermally Carbonized Sewage Sludge and Oxalate Via Molecular Oxygen Activation. Environ. Sci. Technol. 52(21), 12656-12666.

Diaz-Uribe, C. E., Daza, M. C., Martínez, F., Páez-Mozo, E. A., Guedes, C. L. B., Di Mauro, E., 2010. Visible light superoxide radical anion generation by tetra(4-carboxyphenyl)porphyrin/TiO2: EPR characterization. J. Photochem. Photobiol. A: Chem. 215(2), 172-178.

Du, J., Qv, M., Qv, W., Liu, L., Zhang, Y., Cui, M., Zhang, H., 2021. Potential threats of zeolitic imidazolate framework-8 nanoparticles to aquatic fungi associated

with leaf decomposition. J. Hazard. Mater. 401, 123273.

Fettouhi, M., Wazeer, M. I. M., Isab, A. A., 2007. Zinc halide complexes of imidazolidine-2-thione and its derivatives: X-ray structures, solid state, solution NMR and antimicrobial activity studies. J. Coord. Chem. 60(4), 369-377.

Finkelstein, E., Rosen, G. M., Rauckman, E. J., 1982. Production of hydroxyl radical by decomposition of superoxide spin-trapped adducts. Mol. Pharmacol. 21(2), 262-265.

Franklin, N. M., Rogers, N. J., Apte, S. C., Batley, G. E., Gadd, G. E., Casey, P. S., 2007. Comparative Toxicity of Nanoparticulate ZnO, Bulk ZnO, and ZnCl2 to a Freshwater Microalga (Pseudokirchneriella subcapitata): The Importance of Particle Solubility. Environ. Sci. Technol. 41(24), 8484-8490.

Gopal, K., Tripathy, S. S., Bersillon, J. L., Dubey, S. P., 2007. Chlorination byproducts, their toxicodynamics and removal from drinking water. J. Hazard. Mater. 140(1-2), 1-6.

Guo, Y.-F., Fang, W.-J., Fu, J.-R., Wu, Y., Zheng, J., Gao, G.-Q., Chen, C., Yan, R.-W., Huang, S.-G., Wang, C.-C., 2018. Facile synthesis of Ag@ZIF-8 core-shell heterostructure nanowires for improved antibacterial activities. Appl. Surf. Sci. 435, 149-155.

Huang, W.-J., Fang, G.-C., Wang, C.-C., 2005. The determination and fate of disinfection by-products from ozonation of polluted raw water. Sci. Total Environ. 345(1), 261-272.

Jiao, L., Wang, Y., Jiang, H.-L., Xu, Q., 2018. Metal–Organic Frameworks as Platforms for Catalytic Applications. Adv. Mater. 30(37), 1703663.

Jing, H.-P., Wang, C.-C., Zhang, Y.-W., Wang, P., Li, R., 2014. Photocatalytic degradation of methylene blue in ZIF-8. RSC Advances. 4(97), 54454-54462.

Joseyphus, R. S., Nair, M. S., 2008. Antibacterial and Antifungal Studies on Some Schiff Base Complexes of Zinc(II). Mycobiology. 36(2), 93-98.

Kim, S., Choi, W., 2002. Dual Photocatalytic Pathways of Trichloroacetate Degradation on TiO2: Effects of Nanosized Platinum Deposits on Kinetics and Mechanism. J. Phys. Chem. B. 106(51), 13311-13317.

Kohsari, I., Shariatinia, Z., Pourmortazavi, S. M., 2016. Antibacterial electrospun chitosan-polyethylene oxide nanocomposite mats containing ZIF-8 nanoparticles. Int. J. Biol. Macromol. 91, 778-788.

Lee, H., Zhou, B., Liang, W., Feng, H., Martin, S. E., 2009. Inactivation of Escherichia coli cells with sonication, manosonication, thermosonication, and manothermosonication: Microbial responses and kinetics modeling. J. Food Eng. 93(3), 354-364.

Li, M., Zhu, L., Lin, D., 2011. Toxicity of ZnO Nanoparticles to Escherichia coli: Mechanism and the Influence of Medium Components. Environ. Sci. Technol. 45(5), 1977-1983.

Li, P., Li, J., Feng, X., Li, J., Hao, Y., Zhang, J., Wang, H., Yin, A., Zhou, J., Ma, X., Wang, B., 2019. Metal-organic frameworks with photocatalytic bactericidal activity for integrated air cleaning. Nat Commun. 10(1), 2177.

Li, R., Chen, T., Pan, X., 2021. Metal–Organic-Framework-Based Materials for Antimicrobial Applications. ACS Nano. 15(3), 3808-3848.

Liebel, F., Kaur, S., Ruvolo, E., Kollias, N., Southall, M. D., 2012. Irradiation of Skin with Visible Light Induces Reactive Oxygen Species and Matrix-Degrading Enzymes. J. Invest. Dermatol. 132(7), 1901-1907.

Mai-Prochnow, A., Clauson, M., Hong, J., Murphy, A. B., 2016. Gram positive and Gram negative bacteria differ in their sensitivity to cold plasma. Sci. Rep. 6(1),

38610.

Martínez-Huitle, C. A., Brillas, E., 2021. A critical review over the electrochemical disinfection of bacteria in synthetic and real wastewaters using a boron-doped diamond anode. Curr. Opin. Solid State Mater. Sci. 25(4), 100926.

Minero, C., Mariella, G., Maurino, V., Vione, D., Pelizzetti, E., 2000. Photocatalytic Transformation of Organic Compounds in the Presence of Inorganic Ions. 2. Competitive Reactions of Phenol and Alcohols on a Titanium Dioxide−Fluoride System. Langmuir. 16(23), 8964-8972.

Mogana Das, M., Patchamuthu, R., 2016. Sample Preparations for Scanning Electron Microscopy – Life Sciences. Modern Electron Microscopy in Physical and Life Sciences. J. Milos and K. Robert. Rijeka, IntechOpen: Ch. 8.

Moon, J., Yun, C. Y., Chung, K.-W., Kang, M.-S., Yi, J., 2003. Photocatalytic activation of TiO2 under visible light using Acid Red 44. Catal. Today. 87(1), 77-86.

Nieuwenhuijsen, M. J., Toledano, M. B., Eaton, N. E., Fawell, J., Elliott, P., 2000. Chlorination disinfection byproducts in water and their association with adverse reproductive outcomes: a review. Occup. Environ. Med. 57(2), 73.

Nosaka, Y., Nosaka, A. Y., 2017. Generation and Detection of Reactive Oxygen Species in Photocatalysis. Chem. Rev. 117(17), 11302-11336.

Park, K. S., Ni, Z., Côté, A. P., Choi, J. Y., Huang, R., Uribe-Romo, F. J., Chae, H. K., O'Keeffe, M., Yaghi, O. M., 2006. Exceptional chemical and thermal stability of zeolitic imidazolate frameworks. Proc. Natl. Acad. Sci. 103(27), 10186-10191.

Phan, A., Doonan, C. J., Uribe-Romo, F. J., Knobler, C. B., O'Keeffe, M., Yaghi, O. M., 2010. Synthesis, Structure, and Carbon Dioxide Capture Properties of Zeolitic Imidazolate Frameworks. Acc. Chem. Res. 43(1), 58-67.

Rani, N., Sharma, A., Singh, R., 2013. Imidazoles as promising scaffolds for

antibacterial activity: a review. Mini Rev Med Chem. 13(12), 1812-1835.

Redfern, J., Geerts, L., Seo, J. W., Verran, J., Tosheva, L., Wee, L. H., 2018. Toxicity and Antimicrobial Properties of ZnO@ZIF-8 Embedded Silicone against Planktonic and Biofilm Catheter-Associated Pathogens. ACS Appl. Nano Mater. 1(4), 1657-1665.

Reichle, R. A., McCurdy, K. G., Hepler, L. G., 1975. Zinc Hydroxide: Solubility Product and Hydroxy-complex Stability Constants from 12.5–75 °C. Can. J. Chem. 53(24), 3841-3845.

Ren, R., Zhao, H., Sui, X., Guo, X., Huang, X., Wang, Y., Dong, Q., Chen, J., 2019. Exfoliated Molybdenum Disulfide Encapsulated in a Metal Organic Framework for Enhanced Photocatalytic Hydrogen Evolution. Catalysts. 9(1).

Saliba, D., Ammar, M., Rammal, M., Al-Ghoul, M., Hmadeh, M., 2018. Crystal Growth of ZIF-8, ZIF-67, and Their Mixed-Metal Derivatives. Journal of the American Chemical Society. 140(5), 1812-1823.

Setsukinai, K., Urano, Y., Kakinuma, K., Majima, H. J., Nagano, T., 2003. Development of novel fluorescence probes that can reliably detect reactive oxygen species and distinguish specific species. J. Biol. Chem. 278(5), 3170-3175.

Sud, I. J., Chou, D. L., Feingold, D. S., 1979. Effect of free fatty acids on liposome susceptibility to imidazole antifungals. Antimicrob. Agents Chemother. 16(5), 660-663.

Sun, S., Yang, Z., Cao, J., Wang, Y., Xiong, W., 2020. Copper-doped ZIF-8 with high adsorption performance for removal of tetracycline from aqueous solution. J. Solid State Chem. 285, 121219.

Taheri, M., Ashok, D., Sen, T., Enge, T. G., Verma, N. K., Tricoli, A., Lowe, A., R. Nisbet, D., Tsuzuki, T., 2021. Stability of ZIF-8 nanopowders in bacterial culture

media and its implication for antibacterial properties. Chem. Eng. J. 413, 127511.

Taheri, M., Tsuzuki, T., 2021. Photo-accelerated Hydrolysis of Metal Organic Framework ZIF-8. ACS Mater. Lett. 3(2), 255-260.

Troyano, J., Carné-Sánchez, A., Avci, C., Imaz, I., Maspoch, D., 2019. Colloidal metal–organic framework particles: the pioneering case of ZIF-8. Chem. Soc. Rev. 48(23), 5534-5546.

Urano, Y., Higuchi, T., Hirobe, M., 1996. Substrate-dependent changes of the oxidative O-dealkylation mechanism of several chemical and biological oxidizing systems. Journal of the Chemical Society, Perkin Transactions 2.(6), 1169-1173.

Venna, S. R., Jasinski, J. B., Carreon, M. A., 2010. Structural Evolution of Zeolitic Imidazolate Framework-8. Journal of the American Chemical Society. 132(51), 18030-18033.

Wang, J., Wang, Y., Zhang, Y., Uliana, A., Zhu, J., Liu, J., Van der Bruggen, B., 2016. Zeolitic Imidazolate Framework/Graphene Oxide Hybrid Nanosheets Functionalized Thin Film Nanocomposite Membrane for Enhanced Antimicrobial Performance. ACS Appl. Mater. Interfaces. 8(38), 25508-25519.

Wang, Z., Qi, J., Lu, X., Jiang, H., Wang, P., He, M., Ma, J., 2021. Epitaxially grown MOF membranes with photocatalytic bactericidal activity for biofouling mitigation in desalination. J. Membr. Sci. 630, 119327.

Wazeer, M. I. M., Isab, A. A., Fettouhi, M., 2007. New cadmium chloride complexes with imidazolidine-2-thione and its derivatives: X-ray structures, solid state and solution NMR and antimicrobial activity studies. Polyhedron. 26(8), 1725-1730.

WHO, W. B. G., UNICEF. 2022. State of the world's drinking water, Geneva: World Health Organization.

Xu, Y., Fang, Y., Ou, Y., Yan, L., Chen, Q., Sun, C., Chen, J., Liu, H., 2020. Zinc Metal–Organic Framework@Chitin Composite Sponge for Rapid Hemostasis and Antibacterial Infection. ACS Sustain. Chem. Eng. 8(51), 18915-18925.

Yang, J., Yang, Y. W., 2020. Metal-Organic Frameworks for Biomedical Applications. Small. 16(10), e1906846.

Yang, X., Wen, Z., Wu, Z., Luo, X., 2018. Synthesis of ZnO/ZIF-8 hybrid photocatalysts derived from ZIF-8 with enhanced photocatalytic activity. Inorg. Chem. Front. 5(3), 687-693.

요약 (국문초록)

금속 유기 골격체(MOF: Metal-organic frameworks)는 생물 의학 및 환경 응용 분야에서 상당한 주목을 받고 있다. MOF는 금속이온의 저장과 점진적인 방출을 제공해 그 자체로 항균 능력이 있으며, 다공성 구조 내에 물질을 넣어 운송 및 방출할 수 있다. 이 중 제올라이트와 유사한 구조를 가진 ZIF-8는 다양한 장점들로 인해 많은 연구가 진행되었다. 그러나 광범위한 응용 연구에도 불구하고, ZIF-8의 구체적인 항균 기작에 대한 논의는 불분명하다. 본 연구에서는 ZIF-8의 항균 기작에 대해 기존에 제시되었던 연구를 검토하고, 새로운 기작을 제시함으로써 기존 연구를 반박한다. 전구체의 control 실험과 재료 분석을 통해 ZIF-8의 항균 기작이 단순히 아연 이온과 2-메틸이미다졸 리간드의 방출로만 설명될 수 없음을 밝혔으며, 질량 분석과 자유 리간드 측정 등을 통해 아연 이온과 2-메틸이미다졸, 그리고 박테리아 구조체가 형성하는 새로운 복합체가 ZIF-8의 소독 능력의 핵심임을 밝혔다. 더 나아가 기존에 연구된 적 없는 가시광 조건 하에서의 ZIF-8의 소독 광활성을 확인하고, UV-Vis DRS 분석을 통해 앞서 언급한 Zn-mim-박테리아 복합체가 가시광활성의 원인이 될 수 있음을 제시하였다.

주요어 : 금속유기골격체, ZIF-8, 가시광활성, 미생물 소독, 불균일계 촉매, 박테리아

학 번 : 2021-27894